ADVANCED ELECTRONIC MATERIALS
www.advelectronicmat.de

Switchable Optically Active Schottky Barrier in $La_{0.7}Sr_{0.3}MnO_3/BaTiO_3$/ITO Ferroelectric Tunnel Junction

Alberto Rivera-Calzada, Fernando Gallego, Yoav Kalcheim, Pavel Salev, Javier del Valle, Isabel Tenreiro, Carlos León, Jacobo Santamaría, and Ivan K. Schuller*

One of the most desirable attributes of non-volatile memories and memristors is a fast and non-destructive read out of their resistive state. Prototypical ferroelectric (FE) memories use the bulk photovoltaic response associated to the polarization of FE films to address this requirement by optically sensing binary memory cells. A more advanced type of non-volatile memories is FE tunnel junctions (FTJs). They feature resistive state ratios R_{High}/R_{Low} up to 10^6, with a continuum of resistive states accessible, making them promising candidates for neuromorphic computing applications. A novel approach is presented to achieve the optical sensing of the resistive state in a $La_{0.7}Sr_{0.3}MnO_3/BaTiO_3$/ITO FTJ, by using the Schottky barrier forming in the $La_{0.7}Sr_{0.3}MnO_3/BaTiO_3$ interface to dramatically enhance the optical response of the 5 nm $BaTiO_3$ (BTO) barrier. Illumination with UV light exceeding the BTO bandgap through the top transparent ITO electrode generates a photovoltaic response in the R_{High} state, with an open circuit voltage V_{oc} of 400 mV at 20 K, enabling the optical sensing of the resistive state. In the R_{Low} state, the Schottky barrier is removed and the photoresponse disappears.

1. Introduction

Ferroelectric (FE) interfaces are the fundamental building block of devices for a vast number of applications, including but not limited to non-volatile memories, solar cells, and brain-inspired electronics. Accordingly, the intense research efforts of the last years in FE heterostructures are reporting advances in the quest of a universal solid state memory based on FE[1–5] and multiferroic tunnel junctions,[6–11] in the improvement of photovoltaic devices for clean power generation,[12–16] and in the implementation of memristors for neuromorphic computing.[17–20] Most of these research relies on high quality thin film FEs, which benefitted from the great development of growth techniques in the last decades.[21] Typically, these FE layers are sandwiched between two metallic electrodes that permit applying strong electric fields.

Tunneling across thin FE layers allows development of arguably the most promising FE memories: the FE tunnel junction (FTJ). FTJs provide non-volatile resistive switching (RS) with possibility for high-density integration and non-destructive readout. The tunnel barrier can be modulated by an applied voltage producing a non-volatile switch between a high (R_{High}, OFF), and a low resistance state (R_{Low}, ON), in what is called tunneling electro resistance.[22] Extensive research on different materials for the FE barrier and for the metal electrodes resulted in enhanced tunneling electro resistance ratios, R_{High}/R_{Low}, as high as 10^6; the combination of $La_{0.7}Sr_{0.3}MnO_3$ (LSMO) and $BaTiO_3$ (BTO) being one of the most successful choices.[2,4–9,22] In these works, the electro resistance is explained in terms of the different screening lengths of the electrodes, that produces a change in the tunnel barrier profile by the FE polarization reversal, determining the electronic transport of the tunnel junction. A partial polarization inversion via domain formation also enables a continuum of resistance states between R_{High} and R_{Low}, converting FTJ into one of the most interesting implementations of memristors.[17,18,20] A similar tunneling electro resistance and memristor behavior is observed in capacitor structures with insulators based on non-FE transition metal oxides, like colossal magnetoresistive $Pr_{0.7}Ca_{0.3}MnO_3$,[23] Cr-doped $SrZrO_3$,[24] and $SrTiO_3$ (STO).[25] A bipolar switching of the resistance occurs at the interface between the metal

Dr. A. Rivera-Calzada, Dr. F. Gallego, I. Tenreiro, Prof. C. León, Prof. J. Santamaría
GFMC
Universidad Complutense de Madrid
Madrid 28040, Spain
E-mail: alberto.rivera@ucm.es
Dr. Y. Kalcheim,[+] Dr. P. Salev, Dr. J. del Valle,[++] Prof. I. K. Schuller
Department of Physics and Center for Advanced Nanoscience
University of California-San Diego
La Jolla, CA 92093, USA
The ORCID identification number(s) for the author(s) of this article can be found under https://doi.org/10.1002/aelm.202100069.
[+]Present address: Faculty of Materials Science and Engineering, Technion – Israel Institute of Technology, Haifa, 32000, Israel
[++]Present address: Department of Quantum Matter Physics, University of Geneva, 24 Quai Ernest-Ansermet, Geneva, Switzerland

DOI: 10.1002/aelm.202100069

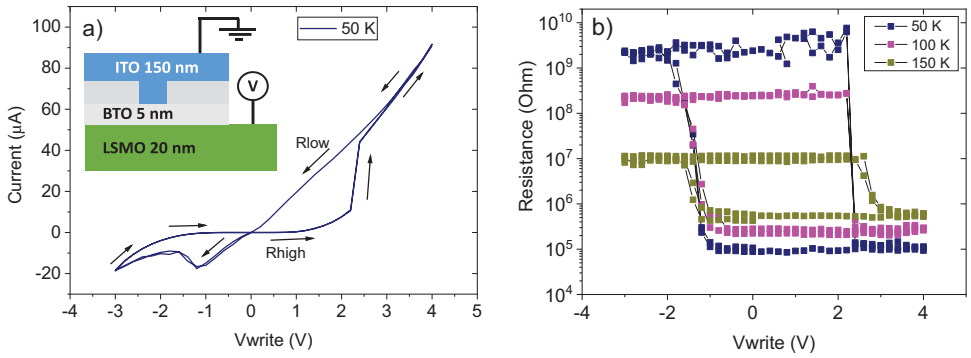

Figure 1. a) Two consecutive *I–V* loops for a 5 nm BTO tunnel junction at 50 K showing the resistive switching. The inset is a side view and electrical connections of the device. b) Two consecutive resistive switching loops (R vs V_{write}) showing the R_{High} and R_{Low} values for each temperature at 50, 100, and 150 K. The resistance state is read with V_{read} = 100 mV.

electrode and the oxide, frequently due to migration of oxygen vacancies and the formation of a Schottky barrier near the electrode.[11,20,26–31] A migration that is observed to enhance inserting an ITO layer acting as a reservoir of the oxygen vacancies.[32] FTJs with the LSMO/BTO interface are reported to display both transport mechanisms at different voltage ranges: a contribution from the oxygen vacancies diffusion in the BTO layer because of the inherent oxygen vacancies concentration of the growth process, and a contribution from the polarization reversal of the BTO.[31] FTJ based on the same LSMO/BTO bilayers as this work (with Ag as a top electrode) were probed by detailed AC and DC electronic transport, PFM, and microscopic characterization with STEM and EELS, with unit cell mapping of the FE polarization displacements. The study evidenced the occurrence of RS due to a Schottky barrier formation by the accumulation of ionized oxygen vacancies in the LSMO/BTO interface, which is facilitated by the FE polarization pointing up (away from the interface).[33–35] The oxygen vacancies accumulation mechanism naturally allows a continuous modulation of the electro resistance of the device, because it can be interrupted at any voltage. The memristor characteristic of our samples is shown in the minor resistance versus V_{write} loops of Figure S10, Supporting Information, of ref. [35], and in agreement with previous works from other groups.[20,31,35]

Schottky barriers in FE materials are known to increase their very attractive photovoltaic effect.[12–16,36–38] FE photovoltaic devices are characterized by a diode-like electric transport with a photocurrent in the opposite direction to the FE polarization. Applying high enough field the polarization is reversed and so is also the direction of the photocurrent, as shown in works on single crystals and thin films.[12–16,36–38] But when the bulk effect is boosted with a proper Schottky barrier, and the FE layer thickness is decreased to the depletion width to reduce recombination, the device turns into a solar cell, with a 2.5% power conversion efficiency.[39] FE photovoltaic effect came as an ideal tool to probe the state of FE devices, because it is fast and not only has low power but also it is active. The first result was the optical sensing of the polarization in non-volatile memories based on FE capacitors with 100 nm of $BiFeO_3$,[40] but research on the optical response of thinner FE layers behaving as FTJ with memristor capabilities are still an open issue. A different approach based on a semiconducting bottom electrode with a long depletion length showed the feasibility of the optical sensing in FTJ.[15]

We present here the optical sensing of the resistive state of FTJ based on the Schottky barrier forming in the LSMO/BTO interface. The LSMO/BTO interface is a paradigmatic example in tunnel electro resistance devices because of the properties of both materials, and because of the high quality of the LSMO/BTO interface grown on top of STO substrates, that we can achieve with the industrially friendly (RF) sputtering.[8,33–35] The ITO top electrode enables the optical access to the FTJ, and also, since oxygen vacancies exist naturally in ITO due to the aliovalent substitution of Sn by In, it acts as a reservoir of oxygen vacancies which can be reversibly exchanged.[32] Our LSMO/BTO/ITO device shows electro resistance ratios in dark comparable to the best devices reported with a R_{High}/R_{Low} over 10^5 below 75 K. Under the 375 nm laser illumination the R_{High} (OFF) state shows a strong photovoltaic effect originating from the Schottky barrier. By removing the Schottky barrier, switching to the R_{Low} (ON) state removes the photoresponse, enabling the active and non-destructive sensing of the resistance state of the FTJ, thus expanding the application possibilities of this kind of devices.

2. Results and Discussion

In this work a series of FTJ are studied, based on epitaxial bilayers of 20 nm $La_{0.7}Sr_{0.3}MnO_3$ and 5 nm $BaTiO_3$, which were grown on STO substrates using a high pressure RF sputtering in a pure oxygen atmosphere.[8,33–35,41] High resolution electron microscopy STEM imaging and elemental maps, and atomic force microscopy show structurally and chemically atomically sharp interfaces, and one-unit cell terraces in the surface of the BTO layer.[33,34] Piezoelectric force microscopy using both amplitude and phase contrast shows hysteresis loops and FE domain reversal with a few tip volts (see Figure 1 of ref. [35]).[35] Tunnel junctions are fabricated defining eight contact areas of 9×18 μm^2 with optical lithography and depositing 150 ± 10 nm ITO as a top electrode through a shadow mask, at room temperature in a DC magnetron sputtering. Electric transport in dark was characterized with a Keithley 2450 source measure unit grounding the top ITO electrode (inset of **Figure 1**a). Optical response was probed

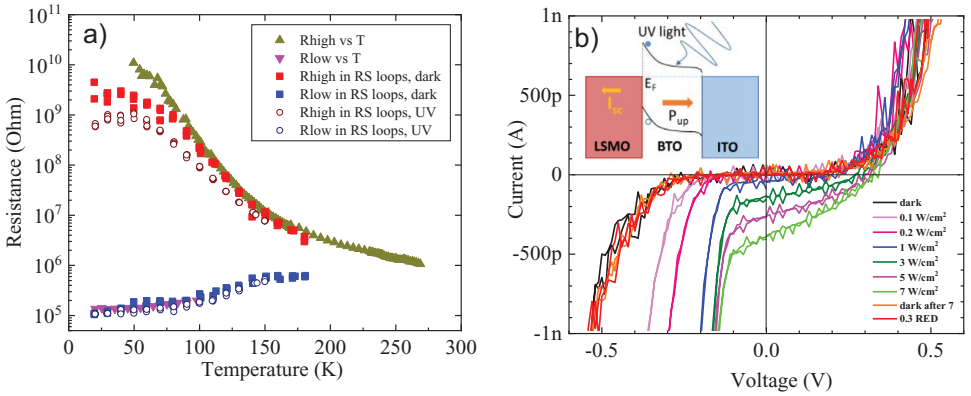

Figure 2. a) Green (up) and magenta (down) triangles are the resistance versus temperature in the R_{high} state and R_{low} state, respectively, measured with a ramp in temperature at 100 mV. Red and blue solid squares are R_{high} and R_{low} as obtained from the RS loops similar to Figure 1b in dark. Wine and navy open circles are R_{high} and R_{low} values from RS loops under 7 W cm^{-2} 375 nm laser illumination. b) *I*–*V* curves at 14 K in the R_{high} state under illumination with increasing power density as specified in the legend, a photovoltaic effect is evidenced above 1 W cm^{-2}. Dark *I*–*V*s before and after UV, and at 0.3 W cm^{-2} red LED illumination (1.9 eV, below BTO bandgap 3.2 eV) are indistinguishable. The inset shows a schematic of the energy bands in the R_{high} state of the FTJ originating a reversed bias photocurrent.

by device illumination with a 375nm laser and a 660 nm LED. More details are given in the Experimental Section.

Figure 1a shows the *I*–*V* characteristic of a LSMO (20nm)/BTO (5 nm)/ITO (150 nm) FTJ at 50 K. The pinched hysteresis loops indicate the occurrence of RS. Note that two consecutive *I*–*V* cycles are almost indistinguishable, showing that the resistive states are highly stable. Above 2.2 V, the device switches from a high resistance diode-like regime to a quasi-Ohmic *I*–*V*. This behavior can be reversed by applying a negative voltage. Figure 1b shows the corresponding two consecutive RS loops (*R* vs V_{write}) of the FTJ at 50, 100, and 150 K. The resistance is measured using a small, non-switching voltage V_{read} = 100 mV to read the resistance set by the writing voltage V_{write}. Since the ITO top electrode is grounded, application of a positive voltage to the bottom LSMO electrode generates an electric field pointing "upwards" (inset of Figure 1a), from the LSMO to the BTO. Figure 1b indicates that positive voltages in the range 2.4–3 V set the low resistance state R_{Low}, and negative voltages in the range –1.6 to –1.8 V reset the high resistance state R_{High}. A low resistance state R_{Low} (ON) is observed after applying an electric field up—pointing toward the BTO/ITO interface—and a high resistance state R_{High} (OFF) is observed after applying a field down—pointing toward the LSMO/BTO interface. This switching pattern rules out the formation of oxygen vacancies filaments, because the coalescence of oxygen vacancies creating the R_{Low} (ON) state is expected under electric fields pointing down, when oxygen vacancies are driven from the ITO into the BTO layer, contrary to what is observed experimentally. Also, the pattern is opposite to the one observed in similar samples when the FE polarization inversion governs the electro resistance. Interestingly, it is reported as the fingerprint of a RS ruled by a Schottky barrier formation due to the migration of oxygen vacancies to the LSMO/BTO interface.[26,31,33–35,42] Therefore, the "chirality" of the *I*–*V* and the RS loops of Figure 1a,b indicates the creation and suppression of a Schottky barrier as the oxygen vacancies accumulate (R_{High}) or are depleted (R_{Low}) at the LSMO/BTO interface, following the external field. Taking into account the LSMO work function W_{LSMO} = 4.8 eV and the BTO electron affinity χ_{BTO} = 3.9 eV, the Schottky–Mott rule estimates a Schottky barrier of ϕ^0_B = 0.9 eV at the LSMO/BTO interface, and a lower ϕ^0_{B2} = 0.6 eV at the BTO/ITO (W_{ITO} = 4.5 eV).

The temperature dependences of R_{High} and R_{Low} states are shown in **Figure 2**a. Magenta down triangles are the R_{Low} values measured with a ramp decreasing temperature in the range 20–100 K, and the blue squares are the R_{Low} values obtained from the RS loops at fixed temperatures (Figure 1b). The R_{Low} state is set with a positive voltage (i.e., the field pointing up), and the values decrease with decreasing temperature in the range 100–20 K, indicating the metallic behavior of the tunnel junction in this state. Moreover, the temperature variation of the resistance in the R_{Low} is similar to the one typically observed in LSMO thin films, showing the low resistance of the BTO barrier and indicating the existence of oxygen vacancies within the FE layer which electron dope BTO into a conductive state. Green up triangles in Figure 2a are the resistance versus temperature in the R_{High} state measured with a ramp increasing temperature (20–180 K) and a voltage of 100 mV, while the red squares are the R_{High} values obtained from the RS loops (Figure 1b) at fixed temperatures. The two values show very good agreement in a wide range of resistances, indicating the robustness of each resistive state. The R_{High} state is reached applying negative voltages (i.e., the field pointing down). In this case, the oxygen vacancies migrate and accumulate in the LSMO/BTO interface, n-type doping the BTO locally and creating band bending of the Schottky barrier. The FTJ in the R_{High} state shows a strong insulator behavior with temperature (Figure 2a), characteristic of a thermally activated transport by thermoionic emission over a Schottky barrier, reaching resistance values in excess of 10^9 Ω below 75 K. Because of the activated temperature dependence, at 300 K the thermal energy facilitates the transport over the barrier and the R_{High} state is very close in resistance to the R_{Low} state, narrowing the R_{High}/R_{Low} ratio. The very different temperature dependences of R_{Low} and R_{High} yield enhanced electro resistance ratios at low temperature,[43] in our samples it increases

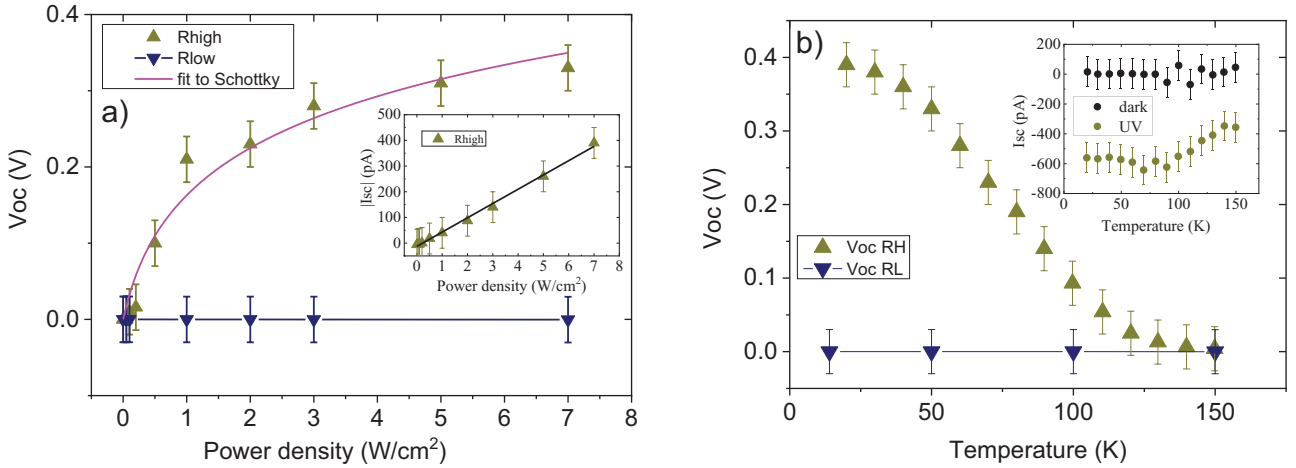

Figure 3. a) Dependence of V_{oc} with the UV laser power at 14 K for R_{high} and R_{low} states. The line is a fit to the Schottky equation $y = A\ Ln\ (1 + x/B)$ accounting for the data. The inset plots I_{sc} versus the laser power density in the R_{high} state with a linear fit to the data. b) V_{oc} versus temperature at 7 W cm^{-2} UV light for R_{high} and R_{low} states, demonstrating the optical sensing of the resistive state. The inset is the temperature dependence of the I_{sc} in the R_{high} state in dark and 7 W cm^{-2} UV light.

over 10^5 below 75 K, reaching values comparable to the best FTJ or memristor devices reported.[17,22]

In the R_{High} state caused by the Schottky barrier, when the sample is irradiated with UV light of energy greater that BTO bandgap, there is a sizable photovoltaic signal which disappears after switching to the R_{Low} state. Figure 2b shows the detailed *I–V* curves of the device under illumination of a 375 nm laser (3.3 eV), at 14 K, in the R_{High} state, at selected light power densities as specified in the legend. A photovoltaic effect is observed above a UV laser power of 1 W cm^{-2}. The plot shows a non-zero current at zero voltage, the short circuit current, I_{sc}; as well as a non-zero voltage at zero current, the open circuit voltage, V_{oc}. Both V_{oc} and I_{sc} are well above the noise background at 1 W cm^{-2}, but indications of a photoresponse are already present at 0.1 W cm^{-2}, with an increased current at negative voltages with respect to the curve in dark. Taking into account that the voltage is applied to the bottom LSMO electrode, a negative I_{sc} implies an injection of photogenerated electrons in the BTO and holes in the LSMO. *I–V*s in dark after and before UV are indistinguishable, showing no device damage due to the laser. Figure 2b also shows that the *I–V* characteristics of our device under a red LED illumination (660 nm, 1.9 eV) are the same as the dark *I–V*. The LED has an estimated power density of 280 mW cm^{-2}, which is almost 50% more power than the 0.2 W cm^{-2} curve from the UV laser in Figure 2b, which shows photoactivity at negative voltages. This implies that photovoltaic response comes from a wide bandgap material like the BTO, which has a bandgap of 3.2 eV, since the top ITO electrode is transparent at this energy. The photovoltaic effect disappears when the resistance state is switched to R_{Low}, the V_{oc} takes negligible negative values (in the mV range), and the I_{sc} becomes positive with big uncertainty due to the low V_{oc}. Since RS modifies only the Schottky barrier of the FTJ that originates the R_{High} state and leaves unaffected the STO substrate, one can rule out the substrate as the origin of the photovoltaic effect. The optical response is originated therefore in the Schottky junction present in the R_{High} state at the high quality LSMO/BTO interface. The built in electric field of the Schottky junction effectively separates the exciton, and the photogenerated current is reversed biased due to the injection of photogenerated electrons in the BTO and LSMO, as depicted in the inset to Figure 2b. Accordingly, a positive V_{oc} and a negative I_{sc} is observed in Figure 2b.

This optical behavior correlates with the buildup and removal of the Schottky barrier when applying negative and positive external fields, accumulating or depleting the LSMO/BTO interface with oxygen vacancies, respectively. In the R_{Low} configuration, vacancies may redistribute in the BTO layer, and/or be partly transferred to ITO across the BTO/ITO interface, but a Schottky response in the top interface is not triggered and the transport is Ohmic-like (energy band diagram in Figure S2, Supporting Information). The Schottky to Ohmic switch observed here is in contrast with the reported situation in bulk FE and thin films with thickness down to 100 nm.[36–40] In these works, the FE polarization inversion determines the RS so the screening charge that generates the Schottky barrier is similar in both electrodes when polarization is reversed, resulting in a symmetric modulation of the Schottky barrier, and V_{oc} and I_{sc} basically change signs.[36–40]

The sign of the I_{sc} is also in agreement with the polarization orientation, since the RS due to migration of oxygen vacancies is reported to appear when the polarization is pointing away from the LSMO/BTO interface.[33–35] In this configuration, the FE polarization facilitates the ionization of oxygen vacancies, and the energy barrier at the LSMO/BTO interface is raised due to the partially unscreened negatively bound polarization charges and the one at the BTO/ITO is lowered due to the positive ones.[15,16,39] The illustration of the energy bands configuration sketched in the inset of Figure 2b shows that both the depolarizing field and the Schottky barrier in the R_{High} state favors photogenerated carrier injection into the electrodes.

In order to investigate the photoresponse, the photogenerated current I_{sc} in the R_{High} state as a function of incident

power is plotted in the inset to **Figure 3**a. The linear increase of I_{sc} with illumination power density implies that it is indeed generated by the UV laser illumination. The increase of V_{oc} with laser power density in the R_{High} state at 14 K is plotted in the main Figure 3a, and the dependence can be accurately described by a logarithmic fit $y = A\ Ln\ (1 + x/B)$. This variation is in agreement with the Schottky equation,

$$V_{oc} = \frac{k_B T}{Nq} Ln\left(1 + \frac{I_{sc}}{I_0}\right) \quad (1)$$

where N is the ideality factor, I_{sc} is the photogenerated current, I_0 is the reversed bias saturation current, and $k_B T/q$ is the thermal voltage. The same expression is valid for the laser power, since I_{sc} is proportional to the illumination power, as shown in the inset. The down triangles in Figure 3a show the V_{oc} in the R_{Low} state is independent of laser illumination. The different behavior of the R_{Low} and R_{High} states enables the determination of the resistive state of FTJ-based memories and memristors by probing the V_{oc} under UV illumination. As an example this device illuminated with a power density of 500 mW cm^{-2} produces a V_{oc} = 0.1 V in the R_{High} state, a high enough voltage for a readout of the high resistance state of a conventional FTJ. This concept provides an easily scalable implementation for low-power optical sensing of multiple devices.

Figure 3b presents the temperature dependence of the V_{oc} in the R_{High} and R_{Low} states under 7 W cm^{-2} UV light. V_{oc} in the R_{High} state decreases monotonically with increasing temperature, from 0.39 ± 0.03 V at 20 K to 4 mV at 150 K. The inset to Figure 3b shows that I_{sc} has a weak dependence with temperature, and at 150 K the FTJ still has I_{sc} = 0.35 nA under 7 W cm^{-2} UV light irradiation. The photovoltaic response usually decreases with increasing temperature due to the rise of recombination rates because of the increased carrier concentrations in semiconductors. Accordingly, the resistance of the BTO in the R_{High} state is reduced over three orders of magnitude as temperature is increased from 50 to 150 K, as shown in Figure 2a, temperature where the V_{oc} vanishes. Considering the circuit model of a photovoltaic device, a decrease in the shunt resistance of the FE layer with increasing temperature explains the decrease in V_{oc} and the relative insensitiveness of the I_{sc} experimentally observed.

In Figure 2a, the open symbols show the R_{High} and R_{Low} values under 7 W cm^{-2} UV laser obtained from the RS loops at the corresponding temperatures. We calculate the resistance in the R_{High} state under UV as the slope of the *I*–*V* curve at 200 mV with respect to the I_{sc} value. UV data are very similar to the values of the dark RS loops in solid squares for R_{Low}, while R_{High} decreases because of the photogenerated carriers (Figure 2a). In addition, the RS loops under UV light do not show any evident change in the switching fields for the RS (Figure S3, Supporting Information). All these facts indicate that the photovoltaic effect appears as an independent parallel mechanism for electronic transport, meaning that in our samples the photogenerated carriers are not interfering with the voltage driven oxygen vacancy migration responsible for the RS. Even though the photovoltaic effect observed is not strong enough in our case to have a V_{oc} at room temperature, the engineering of optically active Schottky barriers in FTJ interfaces appears as a promising route to get active optical sensing of the resistance state in advanced memories and memristors at 300 K.

3. Conclusion

In summary, we studied FTJ based on the LSMO/BTO/ITO layer sequence with a 5 nm thick FE layer. The RS is controlled by creation and removal of a Schottky barrier at the BTO/LSMO interface via field-driven oxygen vacancies migration that is optically active. The Schottky barrier facilitates the separation of photogenerated carriers under 375 nm UV laser irradiation. The reversible build up and removal of an optically active Schottky barrier in the model FE interface LSMO/BTO enables optical sensing of the resistive state and opens a new strategy for the design of parallel, fast, and active readout in solid-state memories and memristors based on FTJ.

4. Experimental Section

Device Fabrication: The FTJ studied were based on epitaxial bilayers of 20 nm $La_{0.7}Sr_{0.3}MnO_3$ and 5 nm $BaTiO_3$, which were grown on (001)-oriented STO substrates using a high pressure RF sputtering in a pure oxygen atmosphere (3.2 mbar).[8,33–35,41] The XRD pattern and reflectivity of the LSMO/BTO bilayer is shown in the Figure S1, Supporting Information. The calculated thickness of the LSMO layer was 19 ± 1 nm, and the BTO one was 5 ± 0.5 nm. A detailed study of the structure of these samples by means of high resolution electron microscopy STEM imaging and elemental maps had been published elsewhere, showing both structurally and chemically atomically sharp interfaces.[33–35] Piezoelectric force microscopy using amplitude and phase contrast on the LSMO/BTO bilayers showed a FE ground state and the possibility to "write" up or down polarization states using a few volts of tip bias.[33–35] Tunnel junctions were fabricated defining eight contact areas of $9 \times 18\ \mu m^2$ with positive photoresist in a Karl Suss MJB3 Mask Aligner. 150 ± 10 nm ITO was deposited as a top electrode through a shadow mask at room temperature in a DC magnetron sputtering. The ratio of the gas in the chamber was 50 sccm Ar and 1 sccm O_2, for a total pressure of 6.2×10^{-3} mbar.

Electrical Measurements: Transport measurements were performed contacting the voltage terminal to the bottom LSMO electrode, and the top ITO electrode to ground. A source meter unit Keithley 2450 was used for the two point electrical characterization. A sketch of the contacts configuration is shown in the inset to Figure 1a. Temperature was swept mounting the sample in a closed cycle He cryostat with optical windows.

Optical Response: The top transparent conducting ITO electrode allowed the authors to optically access the BTO, and the junctions were illuminated using an Oxxius UV LBX-375 nm laser diode (3.3 eV), with an adjustable power supply up to 70 mW and a diameter spot size of 0.7 mm at a distance of 50 mm from the aperture. Power densities were calculated considering a 1 mm^2 laser spot on the sample surface. A red 2 W LED by Thorlabs, model M660L4 with an energy of 1.9 eV (660 nm), below the bandgap of the BTO, was used to ensure the optical response was due to the BTO.

Supporting Information

Supporting Information is available from the Wiley Online Library or from the author.

Acknowledgements

A.R.-C. thanks the economic support of the mobility research program Salvador de Madariaga from Spanish Ministry of Science. Sample fabrication was supported by Spanish AEI through grant MAT2017-87134-C02. This material was based upon the work supported by the Air Force Office of Scientific Research under award number FA9550-20-1-0242.

Conflict of Interest

The authors declare no conflict of interest.

Data Availability Statement

The data that support the findings of this study are available from the corresponding author upon reasonable request.

Keywords

ferroelectric tunnel junctions, optical resistive sensing, photovoltaic effect, resistive switching, Schottky barrier

Received: February 16, 2021
Revised: April 5, 2021
Published online: May 13, 2021

[1] M. Y. Zhuravlev, R. F. Sabirianov, S. S. Jaswal, E. Y. Tsymbal, *Phys. Rev. Lett.* **2005**, *94*, 246802.
[2] C. G. Duan, R. F. Sabirianov, W. N. Mei, S. S. Jaswal, E. Y. Tsymbal, *Nano Lett.* **2006**, *6*, 483.
[3] A. Gruverman, D. Wu, H. Lu, Y. Wang, H. W. Jang, C. M. Folkman, M. Y. Zhuravlev, D. Felker, M. Rzchowski, C.-B. Eom, E. Y. Tsymbal, *Nano Lett.* **2009**, *9*, 3539.
[4] A. Chanthbouala, A. Crassous, V. Garcia, K. Bouzehouane, S. Fusil, X. Moya, J. Allibe, B. Dlubak, J. Grollier, S. Xavier, C. Deranlot, A. Moshar, R. Proksch, N. D. Mathur, M. Bibes, A. Barthélémy, *Nat. Nanotechnol.* **2012**, *7*, 101.
[5] V. Garcia, M. Bibes, *Nat. Commun.* **2014**, *5*, 4289.
[6] M. Gajek, M. Bibes, S. Fusil, K. Bouzehouane, J. Fontcuberta, A. Barthélémy, A. Fert, *Nat. Mater.* **2007**, *6*, 296.
[7] J. P. Veev, C. G. Duan, J. D. Burton, A. Smogunov, M. K. Niranjan, E. Tosatti, S. S. Jaswal, E. Y. Tsymbal, *Nano Lett.* **2009**, *9*, 427.
[8] Z. Sefrioui, C. Visani, M. J. Calderón, K. March, C. Carrétéro, M. Walls, A. Rivera-Calzada, C. León, R. L. Anton, T. R. Charlton, F. A. Cuellar, E. Iborra, F. Ott, D. Imhoff, L. Brey, M. Bibes, J. Santamaria, A. Barthélémy, *Adv. Mater.* **2010**, *22*, 5029.
[9] V. Garcia, M. Bibes, L. Bocher, S. Valencia, F. Kronast, A. Crassous, X. Moya, S. Enouz-Vedrenne, A. Gloter, D. Imhoff, C. Deranlot, N. D. Mathur, S. Fusil, K. Bouzehouane, A. Barthélémy, *Science* **2010**, *327*, 1106.
[10] Y. Wei, S. Matzen, G. Agnus, M. Salverda, P. Nukala, T. Maroutian, Q. Chen, J. Ye, P. Lecoeur, B. Noheda, *Phys. Rev. Appl.* **2019**, *12*, 031001.
[11] V. Rouco, R. El Hage, A. Sander, J. Grandal, K. Seurre, X. Palermo, J. Briatico, S. Collin, J. Trastoy, K. Bouzehouane, A. I. Buzdin, G. Singh, N. Bergeal, C. Feuillet-Palma, J. Lesueur, C. Leon, M. Varela, J. Santamaría, J. E. Villegas, *Nat. Commun.* **2020**, *11*, 658.
[12] M. Qin, K. Yao, Y. C. Liang, *Appl. Phys. Lett.* **2008**, *93*, 16.
[13] T. Choi, S. Lee, Y. J. Choi, V. Kiryukhin, S. W. Cheong, *Science* **2009**, *324*, 63.
[14] I. Grinberg, D. V. West, M. Torres, G. Gou, D. M. Stein, L. Wu, G. Chen, E. M. Gallo, A. R. Akbashev, P. K. Davies, J. E. Spanier, A. M. Rappe, *Nature* **2013**, *503*, 509.
[15] W. J. Hu, Z. Wang, W. Yu, T. Wu, *Nat. Commun.* **2016**, *7*, 10808.
[16] D. J. Kim, M. Alexe, *Appl. Phys. Lett.* **2017**, *110*, 183902.
[17] D. J. Kim, H. Lu, S. Ryu, C. W. Bark, C. B. Eom, E. Y. Tsymbal, A. Gruverman, *Nano Lett.* **2012**, *12*, 5697.
[18] A. Chanthbouala, V. Garcia, R. O. Cherifi, K. Bouzehouane, S. Fusil, X. Moya, S. Xavier, H. Yamada, C. Deranlot, N. D. Mathur, M. Bibes, A. Barthélémy, J. Grollier, *Nat. Mater.* **2012**, *11*, 860.
[19] Y. Yang, X. Zhang, L. Qin, Q. Zeng, X. Qiu, R. Huang, *Nat. Commun.* **2017**, *8*, 15173.
[20] R. Guo, W. Lin, X. Yan, T. Venkatesan, J. Chen, *Appl. Phys. Rev.* **2020**, *7*, 011304.
[21] C. H. Ahn, K. M. Rabe, J.-M. Triscone, *Science* **2004**, *303*, 488.
[22] V. Garcia, S. Fusil, K. Bouzehouane, S. Enouz-Vedrenne, N. D. Mathur, A. Barthélémy, M. Bibes, *Nature* **2009**, *460*, 81.
[23] S. Q. Liu, N. J. Wu, A. Ignatiev, *Appl. Phys. Lett.* **2000**, *76*, 2749.
[24] A. Beck, J. G. Bednorz, C. Gerber, C. Rossel, D. Widmer, *Appl. Phys. Lett.* **2000**, *77*, 139.
[25] Y. Watanabe, J. G. Bednorz, A. Bietsch, C. Gerber, D. Widmer, A. Beck, S. J. Wind, *Appl. Phys. Lett.* **2001**, *78*, 3738.
[26] A. Sawa, *Mater. Today* **2008**, *11*, 28.
[27] S. Tsui, A. Baikalov, J. Cmaidalka, Y. Y. Sun, Y. Q. Wang, Y. Y. Xue, C. W. Chu, L. Chen, A. J. Jacobson, *Appl. Phys. Lett.* **2004**, *85*, 317.
[28] D. Seong, M. Jo, D. Lee, H. Hwang, *Electrochem. Solid-State Lett.* **2007**, *10*, H168.
[29] Y. B. Nian, J. Strozier, N. J. Wu, X. Chen, A. Ignatiev, *Phys. Rev. Lett.* **2007**, *98*, 146403.
[30] S. H. Jeon, B. H. Park, J. Lee, B. Lee, S. Han, *Appl. Phys. Lett.* **2006**, *89*, 042904.
[31] W. Lü, C. Li, L. Zheng, J. Xiao, W. Lin, Q. Li, X. R. Wang, Z. Huang, S. Zeng, K. Han, W. Zhou, K. Zeng, J. Chen, Ariando, W. Cao, T. Venkatesan, *Adv. Mater.* **2017**, *29*, 1606165.
[32] H. J. Kim, M. Kim, K. Beom, H. Lee, C. J. Kang, T. S. Yoon, *APL Mater.* **2019**, *7*, 071113.
[33] G. Sanchez-Santolino, J. Tornos, D. Hernandez-Martin, J. I. Beltran, C. Munuera, M. Cabero, A. Perez-Muñoz, J. Ricote, F. Mompean, M. Garcia-Hernandez, Z. Sefrioui, C. Leon, S. J. Pennycook, M. C. Muñoz, M. Varela, J. Santamaria, *Nat. Nanotechnol.* **2017**, *12*, 655.
[34] J. Tornos, F. Gallego, S. Valencia, Y. H. Liu, V. Rouco, V. Lauter, R. Abrudan, C. Luo, H. Ryll, Q. Wang, D. Hernandez-Martin, G. Orfila, M. Cabero, F. Cuellar, D. Arias, F. J. Mompean, M. Garcia-Hernandez, F. Radu, T. R. Charlton, A. Rivera-Calzada, Z. Sefrioui, S. G. E. te Velthuis, C. Leon, J. Santamaria, *Phys. Rev. Lett.* **2019**, *122*, 037601.
[35] D. Hernandez-Martin, F. Gallego, J. Tornos, V. Rouco, J. I. Beltran, C. Munuera, D. Sanchez-Manzano, M. Cabero, F. Cuellar, D. Arias, G. Sanchez-Santolino, F. J. Mompean, M. Garcia-Hernandez, A. Rivera-Calzada, S. J. Pennycook, M. Varela, M. C. Muñoz, Z. Sefrioui, C. Leon, J. Santamaria, *Phys. Rev. Lett.* **2020**, *125*, 266802.
[36] C. Wang, K. Jin, Z. Xu, L. Wang, C. Ge, H. Lu, H. Guo, M. He, G. Yang, *Appl. Phys. Lett.* **2011**, *98*, 192901.
[37] H. T. Yi, T. Choi, S. G. Choi, Y. S. Oh, S.-W. Cheong, *Adv. Mater.* **2011**, *23*, 3403.
[38] C. J. Won, Y. A. Park, K. D. Lee, H. Y. Ryu, N. Hur, *J. Appl. Phys.* **2011**, *109*, 084108.
[39] Z. Tan, L. Hong, Z. Fan, J. Tian, L. Zhang, Y. Jiang, Z. Hou, D. Chen, M. Qin, M. Zeng, J. Gao, X. Lu, G. Zhou, X. Gao, J.-M. Liu, *NPG Asia Mater* **2019**, *11*, 20.
[40] R. Guo, L. You, Y. Zhou, Z. S. Lim, X. Zou, L. Chen, R. Ramesh, J. Wang, *Nat. Commun.* **2013**, *4*, 1990.

[41] A. Rivera-Calzada, M. R. Diaz-Guillen, O. J. Dura, G. Sanchez-Santolino, T. J. Pennycook, R. Schmidt, F. Y. Bruno, J. Garcia-Barriocanal, Z. Sefrioui, N. M. Nemes, M. Garcia-Hernandez, M. Varela, C. Leon, S. T. Pantelides, S. J. Pennycook, J. Santamaria, *Adv. Mater.* **2011**, *23*, 5268.
[42] Q. H. Qin, L. Äkäslompolo, N. Tuomisto, L. Yao, S. Majumdar, J. Vijayakumar, A. Casiraghi, S. Inkinen, B. Chen, A. Zugarramurdi, M. Puska, S. van Dijken, *Adv. Mater.* **2016**, *28*, 6852.
[43] D. Pantel, M. Alexe, *Phys. Rev. B* **2010**, *82*, 134105.